frontiers | Frontiers in Earth Science

TYPE Original Research
PUBLISHED 21 August 2023
DOI 10.3389/feart.2023.1237367

OPEN ACCESS

EDITED BY
Meng Wang,
Chang'an University, China

REVIEWED BY
Xijun Liu,
Guilin University of Technology, China
Shi Chen,
China University of Petroleum, China

*CORRESPONDENCE
Hao Yang,
gbwfm3@163.com

†These authors have contributed equally to this work

RECEIVED 09 June 2023
ACCEPTED 07 August 2023
PUBLISHED 21 August 2023

CITATION
Yang F, Li J, Lu S, Bian B, Liu H, Wei Y, Qi X and Yang H (2023), Carboniferous to Early Permian tectono-sedimentary evolution in the western Junggar Basin, NW China: implication for the evolution of Junggar Ocean.
Front. Earth Sci. 11:1237367.
doi: 10.3389/feart.2023.1237367

Carboniferous to Early Permian tectono-sedimentary evolution in the western Junggar Basin, NW China: implication for the evolution of Junggar Ocean

Fan Yang[1†], Jianzhong Li[2], Shan Lu[1], Baoli Bian[3], Hailei Liu[3], Yanzhao Wei[1], Xuefeng Qi[1] and Hao Yang[4†*]

[1]PetroChina Research Institute of Petroleum Exploration and Development, Beijing, China, [2]PetroChina Tuha Oilfield Company, Hami, China, [3]PetroChina Xinjiang Oilfield Company, Karamay, China, [4]School of Energy Resources, China University of Geosciences, Beijing, China

The discovery of Carboniferous hydrocarbon source rocks in the Mahu-Shawan Sag has implied considerable exploration potential in the Carboniferous strata in the western Junggar Basin. However, controversy has long surrounded when and how the Junggar Ocean was eventually closed, leading to a poor understanding of the Carboniferous basin evolution and the continental growth of the Central Asian Orogenic Belt. We performed stratigraphic and geochronologic studies to establish the chronostratigraphic framework of the western Junggar Basin to better understand its tectonic-sedimentary evolution during the Carboniferous-Early Permian. Three tectonostratigraphic units in the southern West Junggar region have been identified as Early Carboniferous shallow-deep marine sequences, Late Carboniferous coast-shallow marine sequences, and Early Permian continental sequences. The Carboniferous strata are similar to forearc and backarc-rift sequences in the Western Fault Belt and the Mahu-Shawan Sag, respectively. The Lower Permian strata in the southern West Junggar region are all continental sequences. Seismic profiles indicate extensional settings in the early stage of Late Carboniferous and Early Permian but a compressional setting at the end of Late Carboniferous. Geochemical data have suggested a Carboniferous continental arc setting and an Early Permian within-plate extensional setting. Meanwhile, calc-alkaline arc magma migrated from the Zhongguai High to the Western Fault Belt at the end of the Late Carboniferous. Collectively, the tectonic-sedimentary evolution in the Carboniferous-Early Permian of the southern West Junggar region can be divided into three stages: 1) Early Carboniferous subduction, 2) Late Carboniferous slab roll-back, and 3) Early Permian intra-continental evolution stage. This model constrains the closure of the Junggar Ocean at the Late Carboniferous.

KEYWORDS

basin evolution, western Junggar Basin, forearc basin, backarc basin, closure time, Junggar Ocean

1 Introduction

The Central Asian Orogenic Belt (CAOB; Jahn et al., 2000; Khain et al., 2003; Jahn et al., 2004; Kovalenko et al., 2004; Windley et al., 2007; Cawood et al., 2009; Wilhem et al., 2012; Kroner et al., 2014; Xiao et al., 2015) or Altaids Tectonic Collage (Şengör et al., 1993; Yakubchuk, 2004; Xiao et al., 2008; Wilhem et al., 2012) is the largest accretionary orogen in the world resulted from a complicated collage of various terranes, including ophiolites, island arcs, accretionary complexes, and possibly some microcontinents during the evolution of the Palaeo-Asian Ocean (PAO; Figure 1A). As an important tectonic unit of the southwestern CAOB (Figure 1B), the southern West Junggar region has become a suitable window for exploring the final closure and evolution of the Junggar Ocean (the final remnants of the PAO in southern West Junggar region, Han and Zhao, 2018). In order to investigate the evolution of this ocean, a large number of studies have been carried out on the margins of the western Junggar Basin. However, the closure time and subduction polarity of this ocean are still under debate. The proposed final closure time of the Jungar Ocean varies a lot from the Devonian (Zhu et al., 2013; Zhu et al., 2015), the Early Carboniferous (Han et al., 2010; Xiang, 2015; Tang et al., 2022), the Late Carboniferous (Xu et al., 2013; Li et al., 2017; Zhang et al., 2018a; Zhang et al., 2018b; Zhang et al., 2021), to the Early Permian (Tang et al., 2010; Xiao et al., 2010). In addition, based on the controversy over the subduction polarity, different models of tectonic evolution have been proposed, including the northwestward subduction model (Zhan et al., 2015; Zhang et al., 2018a; Zheng et al., 2019; Liu et al., 2020; Zhang et al., 2021) and the double-sided divergent subduction model (Yin et al., 2013; Eizenhöfer et al., 2015; Yi et al., 2015; Tang et al., 2022). Some breakthroughs suggest that the Zhongguai High in the western Junggar Basin was a volcanic arc during the Carboniferous, which now has been widely recognized (e.g., Li et al., 2014; Li et al., 2017; Zhang et al., 2018a; Zhang et al., 2021). The above controversies have led to the different understandings of the Carboniferous basin attributes of the Mahu-Shawan Sag, with either being a forearc basin in a double-sided divergent subduction model or a backarc basin if it subducted northwestward. The current vague understanding of the Carboniferous basin attributes has led to the debatable formation and development environment of hydrocarbon source rocks in the Mahu-Shawan Sag.

Previous studies mainly focused on the outcropped southern West Junggar, including ophiolite records (e.g., Zhu and Xu, 2006; Chen et al., 2014; Zhu et al., 2015; Zhang et al., 2018a; Zhang et al., 2018b), volcanic rocks (e.g., Gao et al., 2006; Chen and Zhu, 2015; Liu et al., 2017; Zheng et al., 2019) and granitic intrusions (e.g., Yin et al., 2010; Zhang et al., 2015). Comparatively, the tectonic setting, sedimentology and magmatic activities in the buried western Junggar Basin have not been well-constrained. Therefore, this study obtained rich chronological, stratigraphic, tectonostratigraphic, geochemical data in the western Junggar Basin, and then combined the previous studies on the outcrops over the southern West Junggar to reveal the tectonic-sedimentary evolution of the southern West Junggar region in the Carboniferous-Early Permian. This work is of great significance for understanding the formation background of hydrocarbon source rocks in the Mahu-Shawan Sag and the closing process of the Junggar Ocean.

2 Geological setting

2.1 Regional geological background

The West Junggar region, which is a key component of the southwestern CAOB (Windley et al., 2007; Figures 1A,B), includes the West Junggar (West Junggar terrane) and the western Junggar Basin. Based on previous studies of the magmatic and ophiolitic rocks within this orogen, the West Junggar terrane has been separated into the northern and southern domains, which recorded different subduction-accretion histories (Figure 1; Liu et al., 2017; Xu et al., 2013; Zhang et al., 2018b; Zheng et al., 2019; Zhang et al., 2021). The northern West Junggar is bounded by the Irtysh shear zone and the Altai Mountains to the north and the E-W trending Xiemisitial fault zone to the south (Li et al., 2017). It consists of two E-W trending arcs, namely, the Zharma-Saur arc in the north and the Boshchekul–Chingiz arc (also called Xiemisitial arc) in the south, separated by the pre-Carboniferous Kujibai–Hebukesaier–Hongguleleng ophiolitic mélanges (Zhu and Xu, 2006; Zhang and Guo, 2010). The southern West Junggar, separated from northern West Junggar by the Xiemisitai Fault, consists of successive arcs and accretionary complexes dismembered by several left-lateral strike-slip faults, along which two main Late Paleozoic ophiolitic mélanges (Darbut and Karamay) are present. Recent studies have shown that these two main ophiolitic mélanges were controlled by right-lateral shear zones (Zhang et al., 2018a). In this study, we focus on the southern West Junggar region, including the southern West Junggar and western Junggar Basin (Figure 1B).

Taken the pre-Permian strata as the basement and considering the uplift and depression structures of the basement, the first-order structural units of the Junggar Basin can be divided into five tectonic units, namely, the Wulungu Depression, Luliang Uplift, Central Depression, Western Uplift, and East Uplift (Yang et al., 2004). And the second-order tectonic units are divided based on alteration and differentiation of the late tectonic movement. The first-order tectonic units of the western Junggar Basin, our study area, include the Western Uplift and Central Depression. The second-order tectonic units in the Western Uplift include the Hongche Fault Belt, Kebai Fault Belt, Wuxia Fault Belt, and Zhongguai High, while the second-order tectonic units in the Central Depression include Mahu Sag, Dabasong High, Shawan Sag and Pen1jingxi Sag. To facilitate our research, we divided the research area into three units, namely, the Western Fault Belt (WFB), Zhongguai High (ZGH) and Mahu-Shawan Sag (MSS) (Figure 1B).

2.2 Stratigraphic successions of the southern West Junggar region

The strata in the southern West Junggar include the Early Carboniferous Baogutu and Xibeikulasi Formations (C_1b and

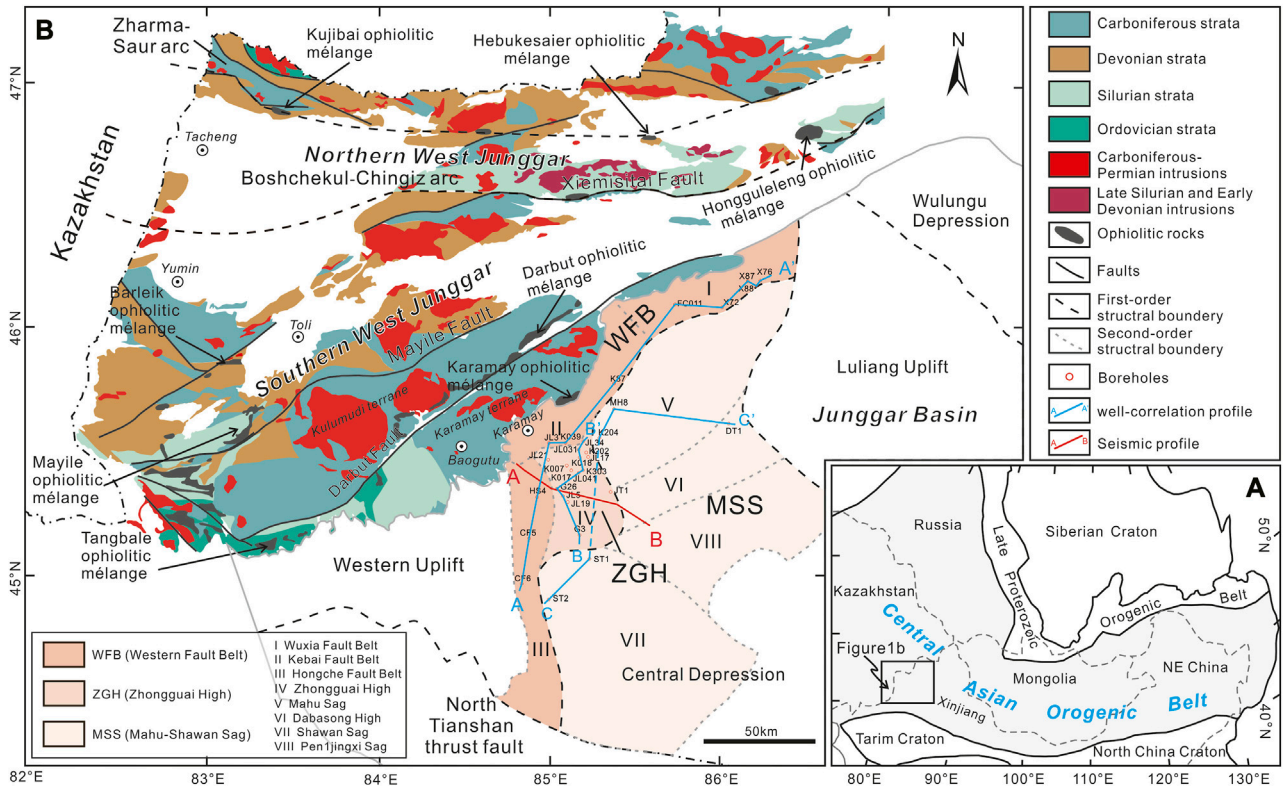

FIGURE 1
Relationship of the study area to the Central Asian Orogenic Belt (modified from Jahn, et al., 2004; Windley, et al., 2007). **(B)** Simplified geological map of the western Junggar Basin and adjacent southern West Junggar showing their tectonic subdivisions and representative wells, seismic reflection profile **(A,B)** location and study areas (modified from Li et al., 2017; Liu et al., 2017; Zhang et al., 2018a; 2021).

C_1x), Late Carboniferous Chengjisihanshan, Hala'alate and Aladeyikesai Formations (C_2c, C_2h and C_2al). The Baogutu and Xibeikulasi Formations are characterized by a set of fine-grained sediments, including siliciclastic rocks, tuffaceous siltstones and volcanic rocks, and mostly developed Bouma sequences (Xiang, 2015). The sedimentary structures and biostratigraphic studies indicate that these Formations formed in a shelf-littoral environment. The Chengjisihanshan Formation (C_2c) unconformably overlying the Baogutu (C_1b) and Xibeikulasi (C_1x) Formations are mainly composed of siltstone and siliciclastic rocks with volcanic rocks interspersed, and their sedimentary structures and biostratigraphic studies indicate a shallow marine environment. The Hala'alate Formation (C_2h) above the Chengjisihanshan Formation mainly contains basalt and andesite, with some continental clastic rocks dominated by sandstone and sand conglomerate, indicating a gradual shallowing of the sea during this period. The Aladeyikesai Formation (C_2al) is overlying the Hala'alate Formation has an increased proportion of continental clastic rocks that mainly include sandstones and siltstones. Their sedimentary structures and biostratigraphic studies indicate this formation formed in a shallow-coastal environment (Figure 4). By contrast, the Lower Permian is characterized by terrestrial deposition.

Three cross-sections were constructed across the western Junggar Basin based on the drilling core data obtained this study (Figure 1B). The WFB is characterized by several foreland thrust belts (He et al., 2004), which formed in the Triassic and early Jurassic (Feng et al., 2008; Feng et al., 2019). The strata in this area include the Lower Carboniferous, Upper Carboniferous, and Lower Permian Jiamuhe Formation and Fengcheng Formation (P_1j and P_1f). The Early Carboniferous strata was only drilled in well K87 of the Kebai fault belt, and the Upper Carboniferous was mainly drilled in the Hongche fault belt. The Lower Permian was distributed in Hongche, Kebai and Wuxia fault belts, and the drilling shows strata in the Wuxia fault belt are thicker with more varied lithologic units than that in the Hongche and Kebai fault belt (Figure 2A). The Early Carboniferous strata are shallow with well-sorted conglomerate and sand conglomerate interbedded with tuff. The GR and SP curves are relatively flat, mainly box-shaped, representing the coastal environment (Figure 4). The Lower Carboniferous can be divided into two parts. The clastic sedimentary rocks in the lower part are mainly tuffaceous siltstones and sandstones, in which the scouring surface and cross-stratification can be seen in the sandstones (Figures 3G,H), the GR value is high, representing shallow-marine environment (Figure 4). The upper part is mainly composed of glutenites, transitioning to tuffaceous mudstones in the southwest direction, representing a shoreface environment (Figure 4). The Early Permian strata, unconformably overlain by the Late Carboniferous strata, are generally rich in continental clastic rocks with horizontal bedding (Figure 3E). The primary

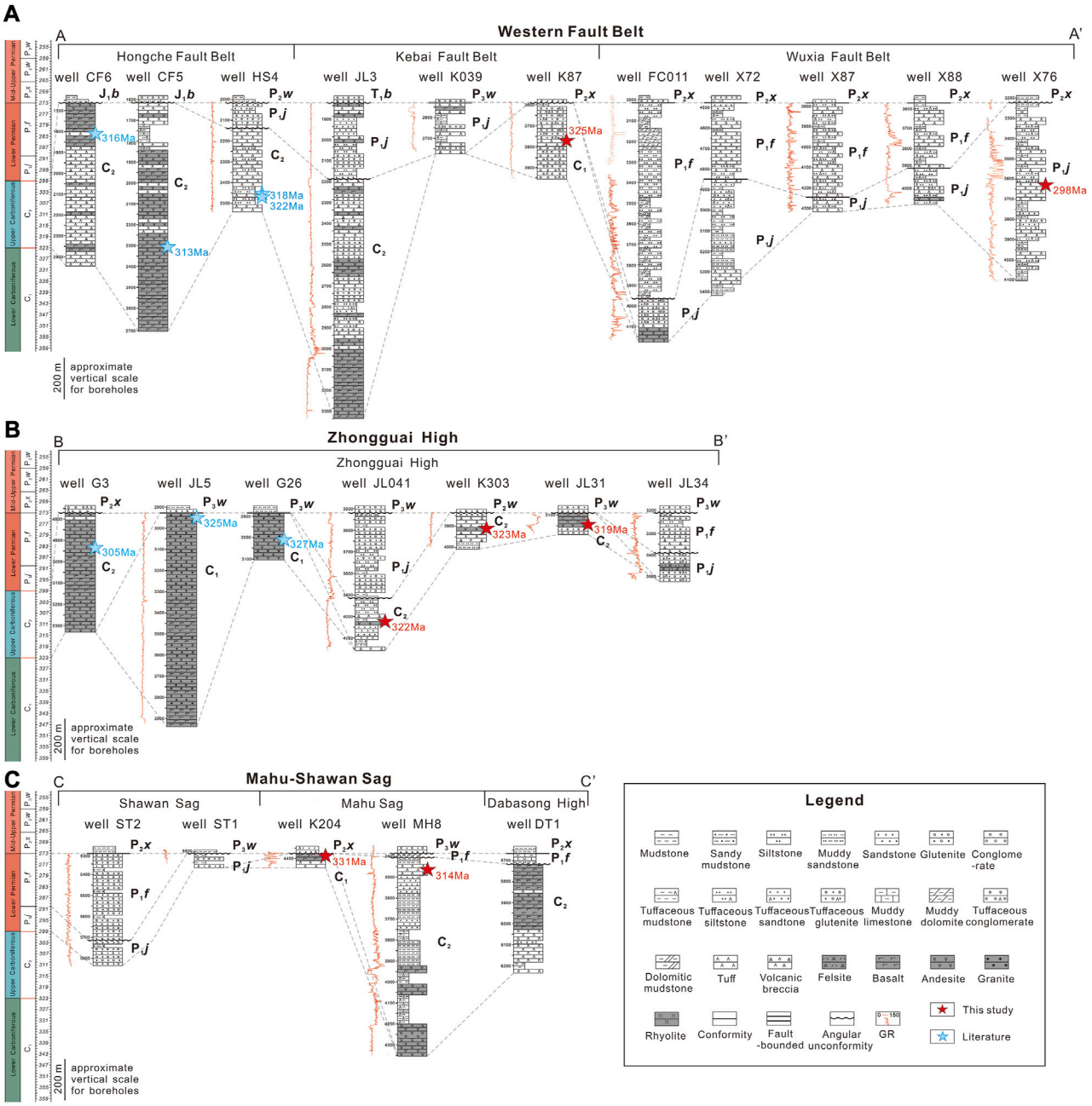

FIGURE 2
Stratigraphic correlation profiles showing the distribution of the Carboniferous-Permian strata in each tectonic unit of the western Junggar Basin.

rock components are tuffaceous mudstones, tuffaceous siltstones layer, tuff, sandstones and andesites. The GR and SP curves are toothed funnel-shaped or bell-shaped, suggesting hydrodynamic variability. They are identified as the lacustrine facies (Figure 4).

The ZGH is characterized by Carboniferous volcanic rocks, while the Early Permian strata were found by drilling in local wells. The Early Carboniferous strata were drilled in wells JL5 and G26 in the center of the ZGH, the Late Carboniferous strata were drilled in wells JL41, K303 and JL31 in the north of the area, and the Early Permian strata were drilled in well JL34 in the north of the area. In general, the Early Permian strata are missing in the southwest of the area but are relatively complete in the northwest part of the ZGH (Figure 2B). The presence of abundant Carboniferous calc-alkaline arc-type volcanic rocks in the ZGH indicates an island arc environment. The overlying Early Permian continental clastic rocks are mainly gray sandy conglomerates, gray siltstones, brown mudstones, gray tuffs and gray volcanic breccias. Load casts and scour surfaces are also identified in the Early and Late Carboniferous strata, respectively (Figures 3I,J). Sawtooth GR and SP curves are box and funnel shaped. These characteristics indicate that the sedimentary facie is fluvial-deltaic facies (Figure 4).

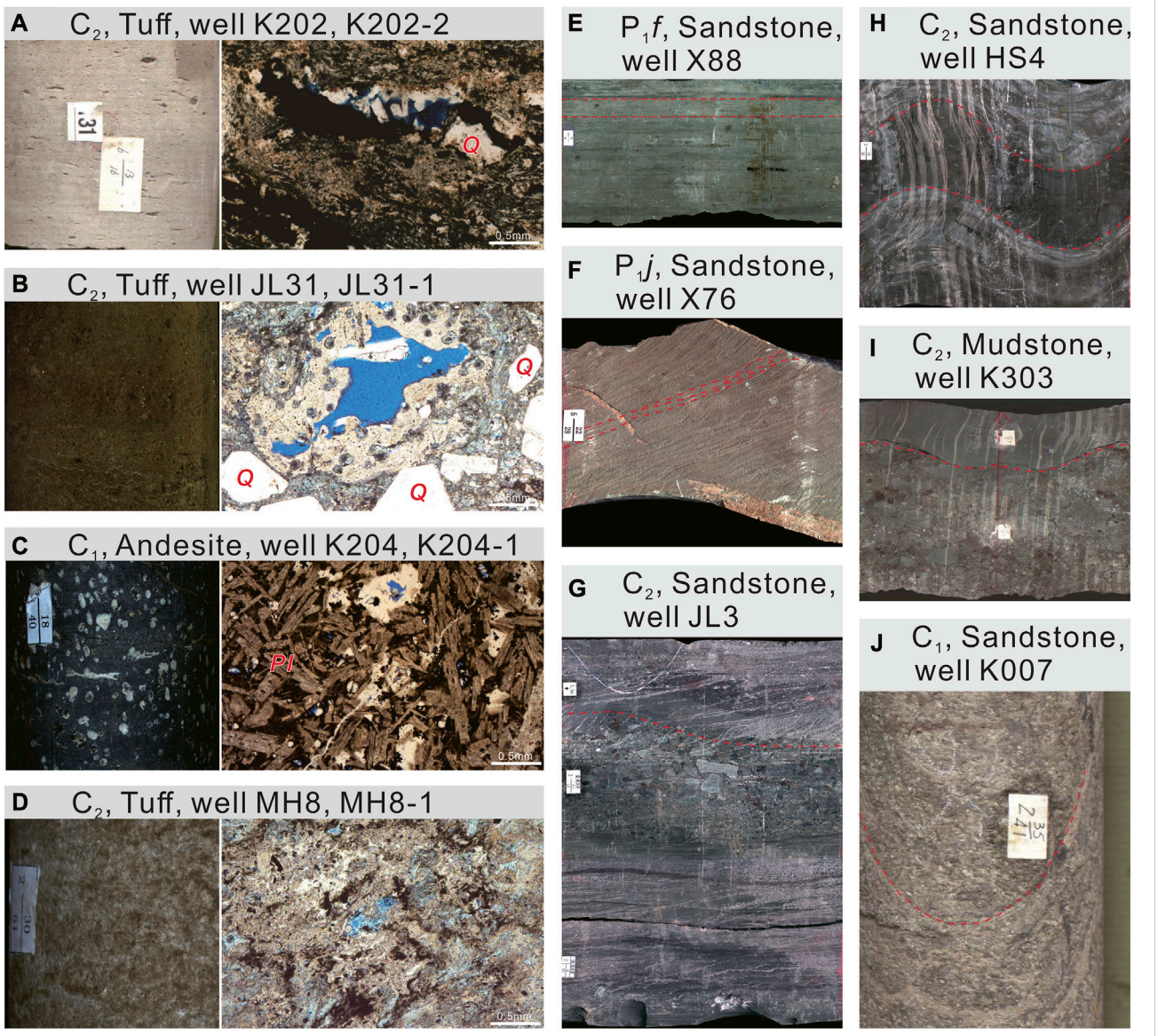

FIGURE 3
Petrological characterisitics and photomicrographs of the Carboniferous-Permian borehole rocks in the western Junggar Basin. **(A)** well K202, 4,169.7 m, C_2, tuff; **(B)** well JL31, 3,148.5 m, C_2, tuff; **(C)** well K204, 4,384.4 m, C_1,andesite; **(D)** well MH8, 3,479.5 m, tuff; **(E)** well X88, 3,830.14–3,830.39 m, P_1j, sandstone, horizontal bedding; **(F)** well X76, P_1j, sandstone, cross-stratification; **(G)** well JL3, 2,132.92–2,133.4 m, C_2, sandstone, scour; **(H)** well HS4, 2,461.30–2,461.64 m, C_2, sandstone and mud, cross-stratification; **(I)** well K303, 3,903.66–3,903.91 m, C_2, mud and glutenite, scour; **(J)** well K007, 3,068.75–3,069.65 m, C_1, sandstone, load cast; Q: quartz; Pl: feldspar.

The distribution of Carboniferous-Early Permian strata in the MSS varies greatly, with the Early Carboniferous strata only drilled in the Mahu Sag' well K204 and Late Carboniferous strata drilled in the Mahu sag and Dabasong high. Strata in the northeast of the Mahu sag and Dabasong high are relatively complete (Figure 2C). The Early Carboniferous strata were drilled in the MSS and mainly consist of dark-gray sandstones, gray basalts, and tuffs, which may represent a coastal environment. The Late Carboniferous strata unconformably overly the Early Carboniferous strata and are mainly composed of fine clastic deposits including tuffaceous mudstones and muddy siltstones, and the GR curve is box-shaped with high value, representing the shallow-marine environment. The Early Permian strata, unconformablly overlying the Late Carboniferous strata, are rich in sandstones and conglomerates, which are considered to be lacustrine facies based on the characteristics of logging curves and previous studies in the MSS (e.g., Tang et al., 2022; Figure 4).

3 Data and methods

This study uses an integrated exploration dataset consisting of geochronological data, wire-line logs, regional seismic profiles and geochemical data, provided by Xinjiang Oilfield, China National Petroleum Corporation (CNPC). Access to many wells and geochronological data allowed us to

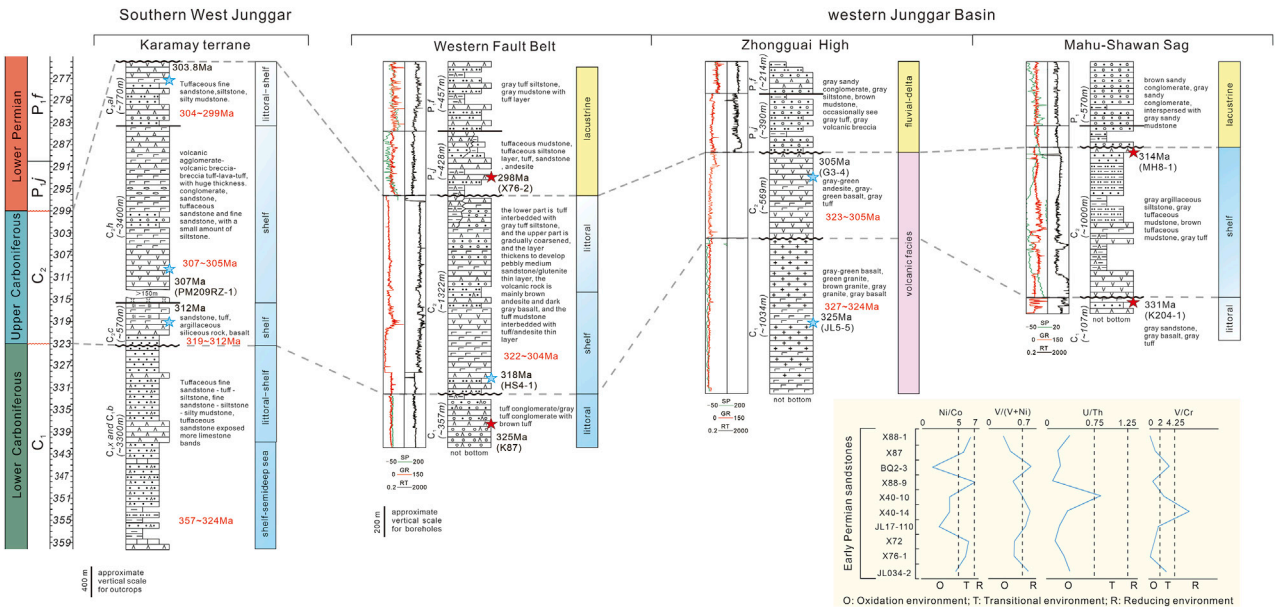

FIGURE 4
Carboniferous to Early Permian stratigraphic columns in the southern West Junggar and in the different tectonic units (WFB, ZGH, MSS) of the western Junggar Basin. Insert diagram shows environments indicated by geochemical data from Early Permian sedimentary rocks.

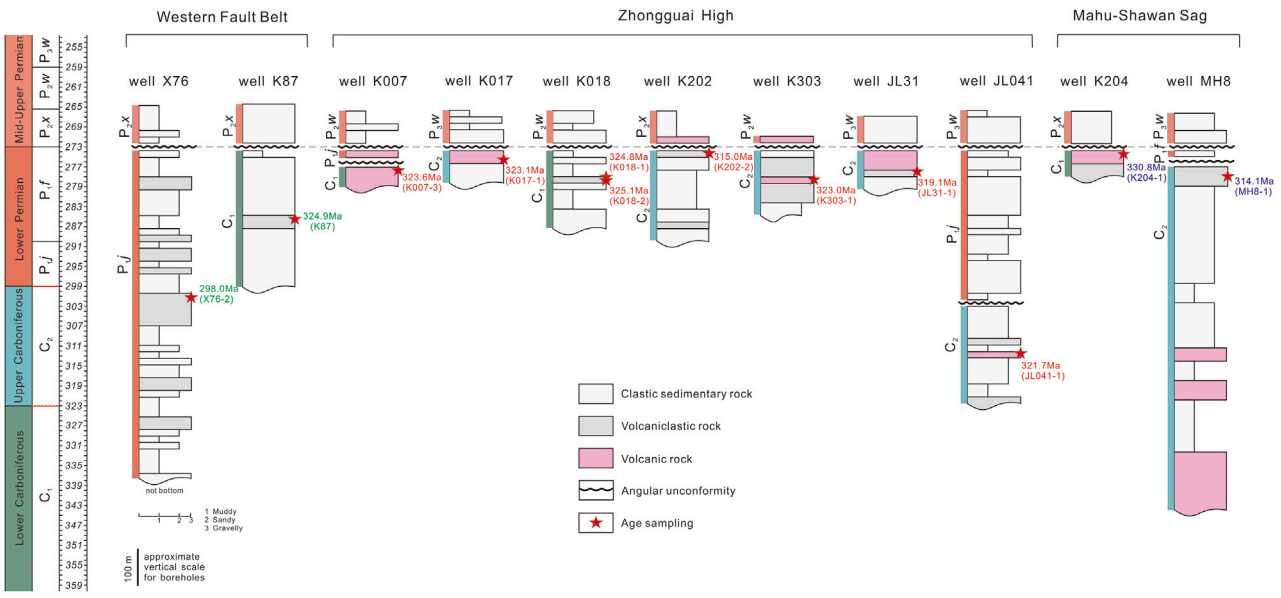

FIGURE 5
Representative stratigraphic column showing the drilled Carboniferous-Permian volcano-sedimentary succession and their sample ages in the western Junggar Basin.

comprehensively reconstruct the stratigraphic sequences of the Carboniferous to Early Permian sedimentary basin in the southern West Junggar region. To determine stratigraphic relationships and to establish the structural framework, we collected seven volcaniclastic and five volcanic rock samples (Figure 5), including two tuff samples from WFB (X76–2 and K87), four tuff samples from ZGH (K018–1, K018–2, K202-2, JL31-1), three andesite samples from ZGH (K017–1, K303-1, JL041-1), one andesitic porphyrite sample from ZGH (K007-3), one tuff sample from MSS (MH8-1), and one andesite sample from MSS (K204-1). Seismic profiles were used to describe the tectonic characteristics and the stratigraphic configuration. In

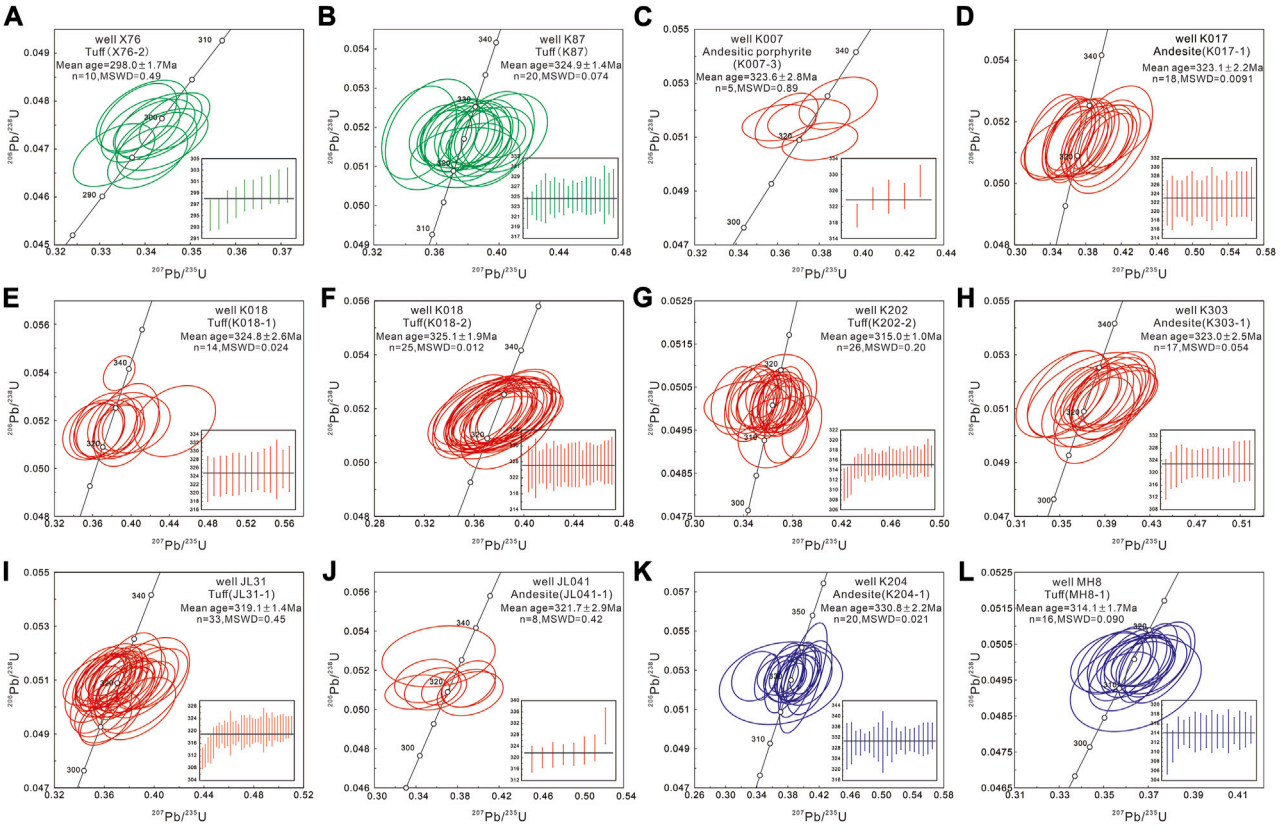

FIGURE 6
Zircon U–Pb concordia diagrams of the borehole volcanic rocks from the Carboniferous-Early Permian strata in the western Junggar Basin.

addition, the large number of whole-rock major and trace element data provide a basis for further investigation of tectonic settings. To summarize, we used geochronological data, analyzed the tectonic deformation characteristics of each period using seismic profiles, and finally used geochemical data to further verify the analysis results. We then established a tectonic-sedimentary evolution model of the Carboniferous-Early Permian in the western Junggar Basin. Taken together, these recent data and geological evidence place critical constraints on the closure history of the Junggar Ocean.

Zircon U-Pb dating were performed by using the laser ablation (multi-collector) inductively coupled plasma mass spectrometer (LA- (MC-) ICP-MS) method at Northwest University in China. Detailed information on sample preparation and analytical procedures is available in the Supporting Material. For U–Pb dating, only one analysis was carried out on each zircon grain.

Major and trace element analyses of the 22 samples were performed at the Analytical Laboratory of the Beijing Research Institute of Uranium Geology, China. Major elements were analyzed by a Philips PW2404 X-ray fluorescence spectrometer. Trace elements of these samples were obtained using a Finnigan MAT high-resolution (HR) inductively coupled plasma mass spectrometer (ICP-MS). The precision and accuracy of the ICP–MS and X-ray fluorescence data were reported by Cullen et al. (2001) and Wu et al. (2010), respectively.

4 Results

4.1 Zircon U–Pb dating

The analyzed zircon grains from all samples show variable U (3-1,294 ppm) and Th (1-1,061 ppm) content with Th/U ratios ranging from 0.26 to 1, indicating a magmatic origin (Williams, 2001; Belousova et al., 2002; Hoskin and Schaltegger, 2003). The U-Pb data are summarized in Figure 6 and Supplementary Table S1.

After excluding the discordant analyses, ten analyses from well X76 tuff (X76-2) from a coherent group define a weighted mean $^{206}Pb/^{238}U$ age of 298.0 ± 1.7 Ma (MSWD = 0.49; Figure 6A). Twenty analyses from well K87 tuff (K87) spread along the concordia in the U-Pb diagram, with $^{206}Pb/^{238}U$ ages clustered from 322 ± 3 Ma to 326 ± 5 Ma, giving a weighted mean age of 324.9 ± 1.4 Ma (MSWD = 0.074) for well K87 tuff (Figure 6B). Five analytical spots from well K007 andesitic porphyrite (K007-3) from a coherent group yield a weight mean $^{206}Pb/^{238}U$ age of 323.6 ± 2.8 Ma (MSWD = 0.89; Figure 6C). Eighteen analytical spots from well K017 andesite (K017-1) are concordant and yield $^{206}Pb/^{238}U$ apparent ages ranging from 322 ± 5 Ma to 324 ± 6 Ma, with a weighted mean age of 323.1 ± 2.2 Ma (MSWD = 0.0091; Figure 6D). Fourteen analytical spots from well K018 tuff (K018-1) have concordant $^{206}Pb/^{238}U$ apparent ages from 323 ± 5 Ma to 326 ± 5 Ma, yielding a weighted mean age of 324.8 ± 2.6 Ma (MSWD = 0.024; Figure 6E). Twenty-five analyses from the well K018 tuff

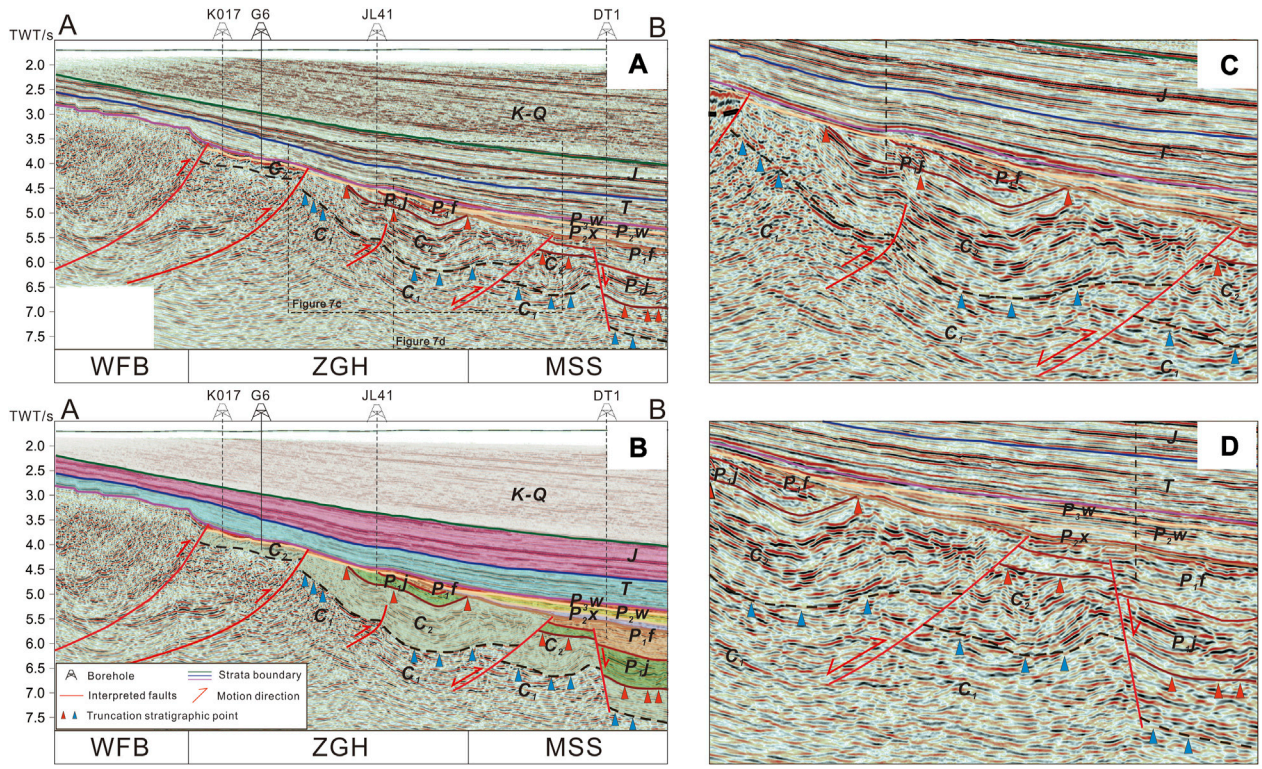

FIGURE 7
(A, B) Seismic profile A-B and their interpretation in the western Junggar Basin. **(C, D)** Enlarged seismic interpretation seismic profile. The primitive seismic profiles were accessed from the Xinjiang oilfield company (CNPC). K-Q, Cenozoic; J, Jurassic; T, Triassic; P_3w, Upper Permian upper-Wuerhe Formation; P_2w, Middle Permian lower-Wuerhe Formation; P_2x, Middle Permian Xiazijie Formation; P_1f, Lower Permian Fengcheng Formation; P_1f, Lower Permian Jiamuhe Formation; C_2, Upper Carboniferous strata; C_1, Lower Carboniferous strata.

(K018-2) cluster on the concordia with concordant $^{206}Pb/^{238}U$ ages ranging from 324 ± 4 Ma to 326 ± 6 Ma, giving a weighted mean age of 325.1 ± 1.9 Ma (MSWD=0.012; Figure 6F). Twenty-six spots from well K202 andesite (K202-2) are concordant and plot on or near the concordia with $^{206}Pb/^{238}U$ apparent ages from 311 ± 3 Ma to 317 ± 2 Ma, giving a weighted mean age of 315 ± 1 Ma (MSWD = 0.20; Figure 4G). Seventeen spots from well K303 andesite (K303-1) have concordant $^{206}Pb/^{238}U$ apparent ages of 318–324 Ma and give a weighted mean age of 323 ± 2.5 Ma (MSWD = 0.054; Figure 6H). Thirty-three spots from well JL31 tuff (JL31-1) have concordant $^{206}Pb/^{238}U$ apparent ages of 311–322 Ma with a weighted mean age of 319.1 ±1.4 Ma (MSWD = 0.45; Figure 6I). Eight analytical spots from well JL041 andesite (JL041-1) are concordant and have $^{206}Pb/^{238}U$ apparent ages of 319–331 Ma, giving a weighted mean age of 321.7 ± 2.9 Ma (MSWD = 0.42; Figure 6J). Twenty analytical spots from well K204 basalt (K204-1) have concordant $^{206}Pb/^{238}U$ apparent ages from 329 to 333 Ma and form a coherent group with a weighted mean $^{206}Pb/^{238}U$ age of 330.8 ± 2.2 Ma (MSWD = 0.021; Figure 4K). Sixteen analytical spots from well MH8 tuff (MH8-1) have concordant $^{206}Pb/^{238}U$ apparent ages of 311–315 Ma and give a weighted mean age of 314.1 ± 1.7 Ma (MSWD = 0.090; Figure 6L). In summary, zircon U-Pb dating suggest the tuffs formed during 325–298 Ma, the andesites formed during 322–323 Ma, one andesitic porphyrite have an age of 323.6 Ma.

4.2 Structural characteristics

Seismic reflection profile A-B (Figure 1B) was employed for understanding the geological structure and structural evolution of the western Junggar Basin. This seismic profile is near NW-SE trending and ~70 km long located within the western Junggar Basin close to the Zaire Mountain. The borehole and log database provide a firm basis for horizon tracing and seismic interpretation as shown in Figure 7. We focus on the interpretation of this seismic section on the Carboniferous and Early Permian strata. The interpretation of the strata after the Early Permian is based on the latest interpretation results of Zhang (2020). For the seismic profile, some truncation stratigraphic points were identified at the interface between the Early Carboniferous and the Late Carboniferous strata, corresponding to the angular unconformity in between. The Late Carboniferous strata are thick near the fault between ZGH and MSS and become thinner toward the west side (Figure 7C). This thrust fault cuts the Late Carboniferous strata and Early Permian strata in the foot wall, and only Late Carboniferous strata remain in the hanging wall. In addition, the seismic profile also reflects more complex deformation in the Late Carboniferous strata compared to in the Early Permian strata in the center of ZGH, indicating a tectonic setting transition from extension to compression at the end of the Late Carboniferous (Figure 7C). In the Early Permian, we identified a southeast normal fault in the MSS and the thickening of the strata

in the foot wall (Figure 7D), indicating they may have formed due to a Permian extension.

4.3 Geochemical characteristics

The analytical geochemical data are listed in Supplementary Table S2. For the following discussion, major elemental data are normalized on an anhydrous basis. Relatively high loss on ignition (LOI = 1.32%–11.20%) indicate that the samples experienced varying degrees of alteration. Therefore, we focus on the immobile and transitional elements (e.g., Zr, Y, Nb, Th, Ti) for rock classification and petrogenetic discussion (Frey et al., 2002).

With exception of sample K204-1, all other Early Carboniferous samples are characterized by their moderate SiO_2 contents (53.92%–65.05%) and relatively low total alkali contents (Na_2O+ K_2O = 3.75%–8.19%), and belong to the andesite/dacite field on the Zr/TiO_2 vs. Nb/Y diagram (Figure 8A). These intermediate-acidic samples have compositions with low $Fe_2O_3^T$ (4.13%–5.33%), MgO (1.14%–2.22%), TiO_2 (0.48%–0.78%), and high Al_2O_3 (13.88%–19.00%). Sample K204-1 exhibits low SiO_2 contents (50.60%), and reatively high $Fe_2O_3^T$ (10.61%), MgO (3.34%), TiO_2 (1.33%). On the Th vs. Co diagram of Hastie et al. (2007) that is affective for altered volcanic rocks, all of these samples are plotted in the calc-alkaline field (Figure 8B). The Late Carboniferous samples can be divided into two groups based on their respective composition characteristics. Group 1 have intermediate-basic compositions with a wide range of SiO_2 (45.14%–68.29%) and low total alkali contents (Na_2O+ K_2O = 2.50–6.87%). The samples have relatively low Al_2O_3 (13.12%–16.18%) and high $Fe_2O_3^T$ (5.01%–7.69%), TiO_2 (0.71%–1.34%), P_2O_5 (0.18%–0.48%) and varying MgO (1.11%–7.20%) and CaO contents (2.95%–9.65%). On the Zr/TiO_2 vs. Nb/Y diagram, the samples plot in the andesite/basalt fields (Figure 8A). Group 2 have intermediate-basic compositions with a narrow range of SiO_2 (66.40%–76.80%) and relatively high total alkali contents (Na_2O+ K_2O = 6.02–7.97%). The samples also have low Al_2O_3 (10.45%–12.04%) and varying Cao contents (0.32%–5.56%), but relatively low $Fe_2O_3^T$ (1.68%–1.86%), TiO_2 (0.09%–0.16%), P_2O_5 (0.03%–0.05%) and MgO contents (0.09%–0.53%). On the Zr/TiO_2 vs. Nb/Y diagram, the samples plot in the rhyolite/comendite fields (Figure 8A). However, the samples both plot in the calc-alkaline field on the Th vs. Co diagram (Figure 8B). With exception of sample X76-2, all other Early Permain samples are characterized by their low SiO_2 contents (55.52%–57.75%) and relatively low total alkali contents (Na_2O+ K_2O = 5.47%–7.69%), and belong to the andesite/dacite field on the Zr/TiO_2 vs. Nb/Y diagram. Sample X76-2 have moderate SiO_2 (58.35%) and total alkali contents (Na_2O+ K_2O = 7.14%), and plot in the rhyolite field on the Zr/TiO_2 vs. Nb/Y diagram (Figure 8A). It also have compositions with relatively high Al_2O_3 (18.83%), MgO (3.35%) and low $Fe_2O_3^T$ (2.83%), TiO_2 (0.18%), and belong to calc-alkaline rhyolite on the Th vs. Co diagram (Figure 8B).

In addition, there are five sedimentary rock samples in this study (X88-1, X87, X72, X76-1, and JL034-2). These rocks show a relatively wide variation in SiO_2 contents (38.31%–74.96%), with an average of 57.64%. The samples have wide ranges of Na_2O (2.06%–4.68%, av. 3.16%) and K_2O (1.36%–4.11%, av. 2.74%). In comparison with the Post-Archean Australian average shale (PAAS) (Taylor and McLennan, 1985), the samples yield lower Al_2O_3 (av. 14.22%) and $Fe_2O_3^T$ (av. 3.67%) and higher MgO contents (2.66%).

5 Discussion

5.1 Carboniferous to Early Permian chronostratigraphic framework in the southern West Junggar region

The rich geochronological data from this study provide firm constraints on the Carboniferous to Early Permian chronostratigraphic framework in the southern West Junggar region. Palaeontological as well as geochronological studies in the Karamay terrane show that the ages of intrusive rocks in the Baogutu Formation are 327–316.9 Ma (Gao et al., 2006; Han et al., 2006; Chen and Zhu, 2015). The geological periods of the fossil assemblage are mainly from the Late Visean to the Bashkirian (e.g., *Pugilis* sp., *Semicostella* sp., *Linoproductus praelongatus*, Xiang, 2015). The volcanic rocks or tuff samples of the Baogutu formation are from 357.5 Ma to 328 Ma (An and Zhu, 2009; Tong et al., 2009; Guo et al., 2010). In addition, the ages of intrusive rocks in the Xibeikulasi Formation are 327–313.7 Ma (Han et al., 2006; Xiang, 2015), and most fossils are in the Early Carboniferous Visean. Although the order of these two formations remain uncertain, the timing of the two formations are well-constrained to the Early Carboniferous within a reasonable range (357–324 Ma, Figure 4). In this study, several borehole volcanic rocks from the western Junggar Basin also gave similar ages of 330.7–324 Ma.

The Upper Carboniferous in the Karamay terrane includes the Chengjisihanshan Formation, the Hala'alate Formation, and the Aladeyikesai Formation, with deposition ages of 319–312 Ma, 307–305 Ma and 304–299 Ma, respectively (Xiang et al., 2013; Xiang et al., 2015; Li et al., 2016; Peng et al., 2016). In the WFB, our chronological data of volcanic rocks suggest depositional ages of 322–304 Ma. In the ZGH, the deposition age are in 323–305 Ma. In MSS, only one volcanic sample gives an age of 314.5 Ma.

The Early Permian strata include the Jiamuhe Formation and Fengcheng Formation, and their ages are 292–273 Ma (Liu, 2015; Lu, 2018; Tang et al., 2021; Tang et al., 2022). In this study, a Permian volcanic rock sample from the well X76 gives an age of 298 Ma.

5.2 Carboniferous arc-basin system of the western Junggar Basin

The southern West Junggar region is a key area to study the Late Paleozoic evolution of the subduction-collision processes of Junggar Ocean (e.g., Xiao et al., 2015; Li et al., 2017; Liu et al., 2017). Combining our detailed stratigrapic and sedimentologic data with seismic reflection features (Figures 4, 7), Carboniferous volcano-sedimentary succession in this region was punctuated by unconformities into aforementioned three main tectonostratigraphic units involving C_1, C_2, and P_1. The ZGH is dominated by Early Carboniferous calc-alkaline arc magmatic

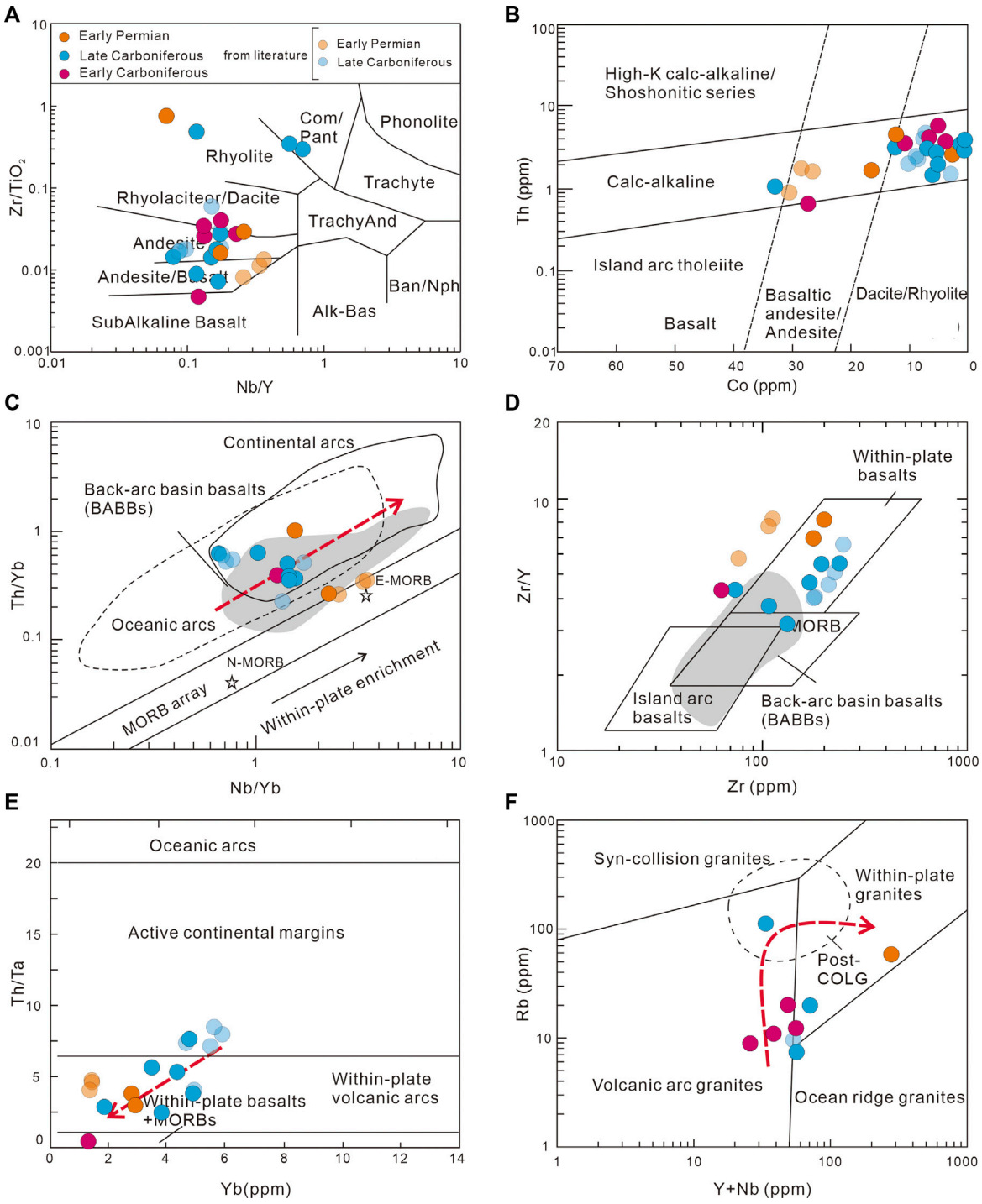

FIGURE 8
Tectonic diacrimination diagrams with trace element plots of the Carboniferous-Early Permian volcanic rocks in western Junggar basin and adjacent areas. **(A)** Zr/SiO_2-Nb/Y diagram (Winchester and Floyd, 1977); **(B)** Th-Co diagram (Hastie et al., 2007); **(C)** Th/Yb-Nb/Yb diagram (Pearce and Peate, 1995; Zhu et al., 2012); **(D)** Zr/Y-Zr diagram (Pearce and Norry, 1979; Zhu et al., 2012); **(E)** Th/Ta-Yb diagram (Gorton and Schandl, 2000); **(F)** Rb-(Y+Nb) diagram (Pearce et al., 1984; Wang et al., 2017). Literature data of the Carboniferous–Early Permian magmatic rocks in the study area are from Yin et al. (2013), Li et al. (2014), and Lu. (2018).

records (Figures 8A,B) and a series of southeastward-vergent thrust faults (Li et al., 2017). Previous studies also have determined the ZGH as an Early Carboniferous island arc (Li et al., 2014; Li et al., 2017; Zhang et al., 2018a; Zhang et al., 2021; Tang et al., 2022), but whether the WFB or MSS is a forearc basin in the Carboniferous remains a key question.

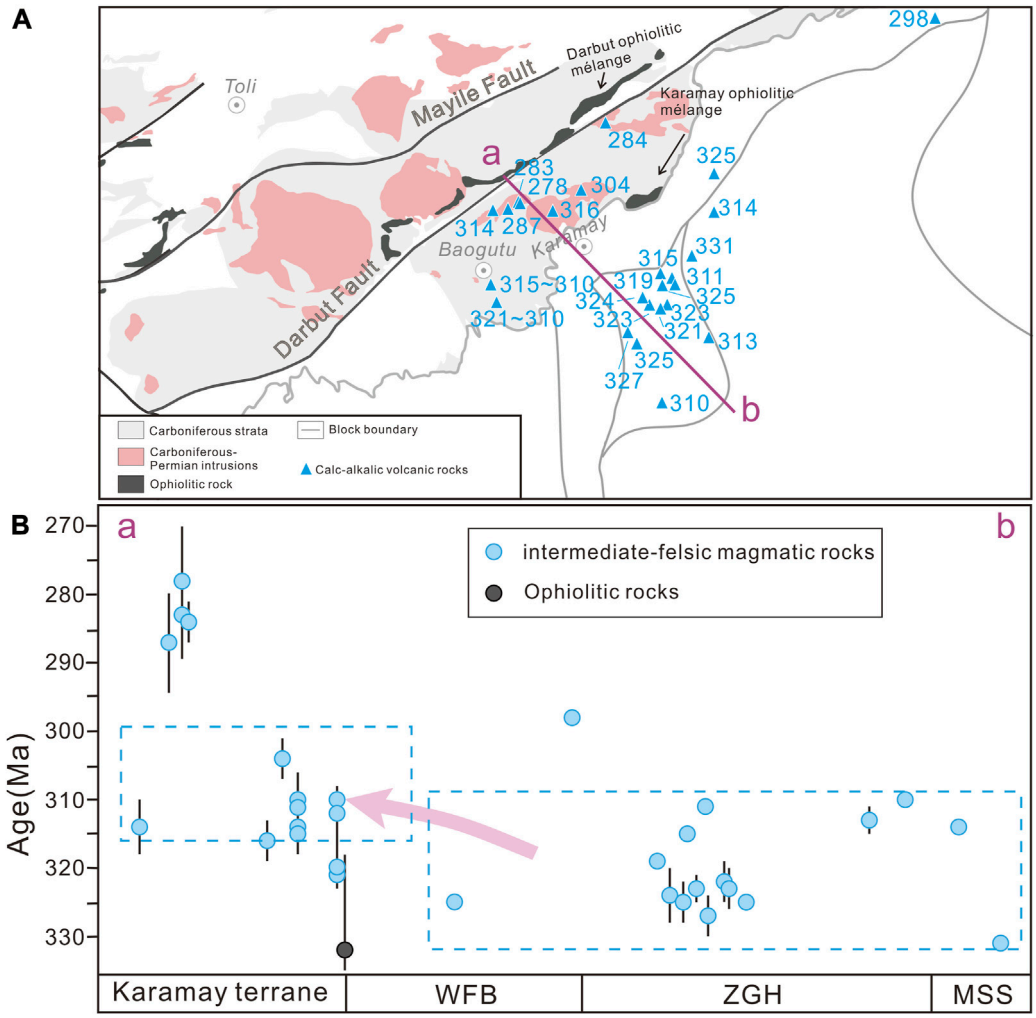

FIGURE 9
Age and distribution **(A)** and migration characteristics **(B)** of the Carboniferous to Early Permian magmatic rocks in the western Junggar Basin and adjacent areas. Literature data of magmatic rocks are from Li et al. (2014), Lu (2018), Cao et al. (2016), Tang et al. (2010), Tang et al., 2021, Yin et al. (2013), and Zhan et al. (2015).

Forearc basins were proposed as sedimentary basins that develop lie between the accretionary prisms and the magmatic arc or superimposed on the accretionary prisms. (Dickinson, 1974; Karig and Sharman, 1975; Dickinson and Seely, 1979; Dickinson, 1995; Noda, 2016). Studies have shown that most of the siliciclastic strata in the forearc basin are derived from igneous rocks produced by arc magmatism and deposited in submarine slope and fan depositional environments (Ingersoll, 1982; Ingersoll and Schweickert, 1986). Typical forearc basin fills shoal upward into shallow-marine or nonmarine strata but is dominated by deep marine strata (e.g., Dickinson, 1995; Busby et al., 1998; Fildani et al., 2008). However, the sedimentary characteristics of modern oceanic arc-related forearc basins have shown that these basins have a massively thick marine sequence, including large sections of pelagic sediments interspersed with thin layers of sandstone or volcanic ash, or large sections of pelagic carbonate rocks (e.g., Kumano basin; Tofino basin). The Carboniferous strata of the WFB was strong affected by tectonic activity after the Middle Permian (Figure 7). Only a relatively coarse-grained set of sediments from Serpukhovian (−324.9 Ma) was drilled in well K87 (Figure 2). However, the similarity between the Late Carboniferous strata of the WFB and the Late Carboniferous strata of the Karamay terrane is obvious (Figure 4). Therefore, the Early Carboniferous stratigraphic information of the Karamay terrane can compensate for the lack of early Carboniferous stratigraphic information in the WFB to a certain extent. The Carboniferous strata of the WFB generally exhibit a sequence of gradually shallowing upward, which conforms to the vertical sedimentary characteristics of forearc basins. The Carboniferous strata under investigation deserve attention because they do not have the same characteristics as the typical forearc basins found in modern oceanic island arcs. Specifically, the strata is lacking in large amounts of mudstone, indicating that they are more likely to be sediments related to a continental island arc forearc basin. Geochemical data also indicate a continental arc attribute during the Carboniferous (Figures 8C,E). In addition, previous studies in the area have found detrital zircons from the ancient crystalline

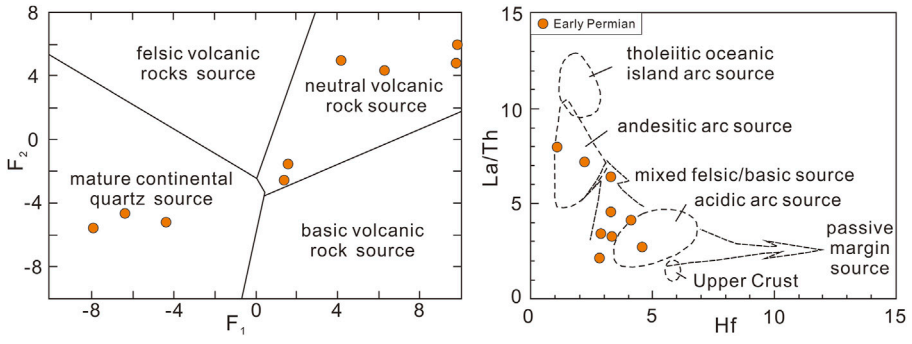

FIGURE 10
Geochemical diagrams showing source variation and composition for the Early Permian sedimentary rocks (Roser and Korsch, 1988). F_1= −1.773*TiO_2+ 0.607*Al_2O_3+ 0.760*Fe_2O_3 − 1.500*MgO + 0.616*CaO + 0.509*Na_2O − 1.224*K_2O − 9.090; F_2= −0.445*TiO_2+ 0.070*Al_2O_3− 0.250*Fe_2O_3− 1.142*MgO+ 0.438*CaO + 1.475*Na_2O + 1.426*K_2O − 6. 861.

basement of the Junggar Basin, suggesting a possible continental island arc (e.g., Li, 2011).

Dickinson (1974) described the sedimentary basins that behind an active volcanic arc as a "retro-arc" basin. Today, the term of "retro-arc basin" refers generally to the compressional regime of the backarc basin, while the extensional or neutral regime of this basin is more often referred to as a "backarc basin." Many backarc basins are extensional in origin, forming by rifting and seafloor spreading (Marsaglia and Ingersoll, 1992). Back-arc rifting is an important process in the evolution of Earth's crust and has been observed in several regions of the world, including the western Pacific Ocean, the South Pacific, and the Andes mountain range in South America. Typically, the sedimentary deposits in backarc basins can be divided into three stages, which reflect changes in the depositional environment and the nature of the sedimentary deposits. These stages are: Initial Rifting Stage: During this stage, the backarc basin is forming as a result of tectonic extension and thinning of the Earth's crust. Sediment is primarily derived from erosion of the surrounding volcanic arc, and is characterized by volcaniclastic deposits, such as ash fall and pyroclastic flow deposits. Transitional Stage: During this stage, the basin continues to evolve and fill with sediment, and the depositional environment becomes more mature and stable. Sediments can include a mixture of volcanic and sedimentary deposits, including volcaniclastics, coarse-grained volcaniclastic sandstones, and shale. Late Stage: During this stage, the backarc basin has reached its maximum size and the rate of sedimentation decreases. The depositional environment becomes dominated by fine-grained sedimentary deposits, such as mudstone, shale, and turbidite sandstone, which are formed by the accumulation of sediment transported by turbidity currents (e.g., Izu-Bonin-Mariana arc; Iizasa et al., 1999; Fiske et al., 2001). Therefore, the filling sequences of the backarc rift basin have many volcanic and volcaniclastic records in the initial rifting stage. As the continue of rifting, the sediment particle size becomes finer during the expansion period and transitioned to deep marine deposition. In the MSS, except that only a thin layer of the Early Carboniferous strata was drilled in well K204, little information is available on the Early Carboniferous strata, limiting the basin study in this area. The Late Carboniferous strata are fine-grained rifting sediments controlled by normal faults (Figures 4, 7). On the Nb/Yb vs. Th/Yb diagram, the vast majority of samples fall in the continental arc field (Figure 8C). Meanwhile, to explore the basin attributes, we delineated the basaltic zone of the backarc basin based on Zhu et al. (2012), and samples from this region falling in the backarc basin basalt (BABB) zone (Figures 8C,D).

In conclusion, the sedimentary characteristics of the Carboniferous show that the WFB area is a gradually shallower sequence, the ZGH area is dominated by calc-alkaline arc magma, and the MSS area is a relatively fine-grained deposit (Figure 4). Based on the above results of sedimentray records, structural features and geochemical characteristics, the southern West Junggar region was a continental arc-basin system during the Carboniferous. At this period, the ZGH was a continental volcanic arc, the WFB was a forearc basin and the MSS was a backarc basin. Combined with the presence of Devonian-Early Carboniferous ophiolites (e.g., Zhang and Huang, 1992; Xu et al., 2006; Yang et al., 2012; Chen et al., 2014; Zhu et al., 2015), we consider that the formation of the arc-basin system in the western Junggar Basin resulted from southward subduction of the Junggar oceanic lithosphere, and the subduction context continued at least to the Late Carboniferous. The temporal and spatial evolution of arc magma reveal a migration pattern from the Zhongguai arc to its forearc area (e.g., WFB and Karamay terrane) at ca. 315–310 Ma (Figure 9), indicating that slab rollback may take place at that time, which is responsible for the Late Carboniferous rifting in the western Junggar Basin and the development of Mahu-Shawan backarc basin.

5.3 Constraint on the closure time of the Junggar Ocean

Given similar occurance of accretionary system in the Kulumudi terrane, our determined southward subduction polarity of the Junggar Ocean provide further support for a divergent double subduction model (Yin et al., 2013). However, the closure time of this oceanic basin is still poorly constrained, with proposals ranging from the Carboniferous to Permian (Han et al., 2006; Tang et al., 2010; Li et al., 2017). The angular

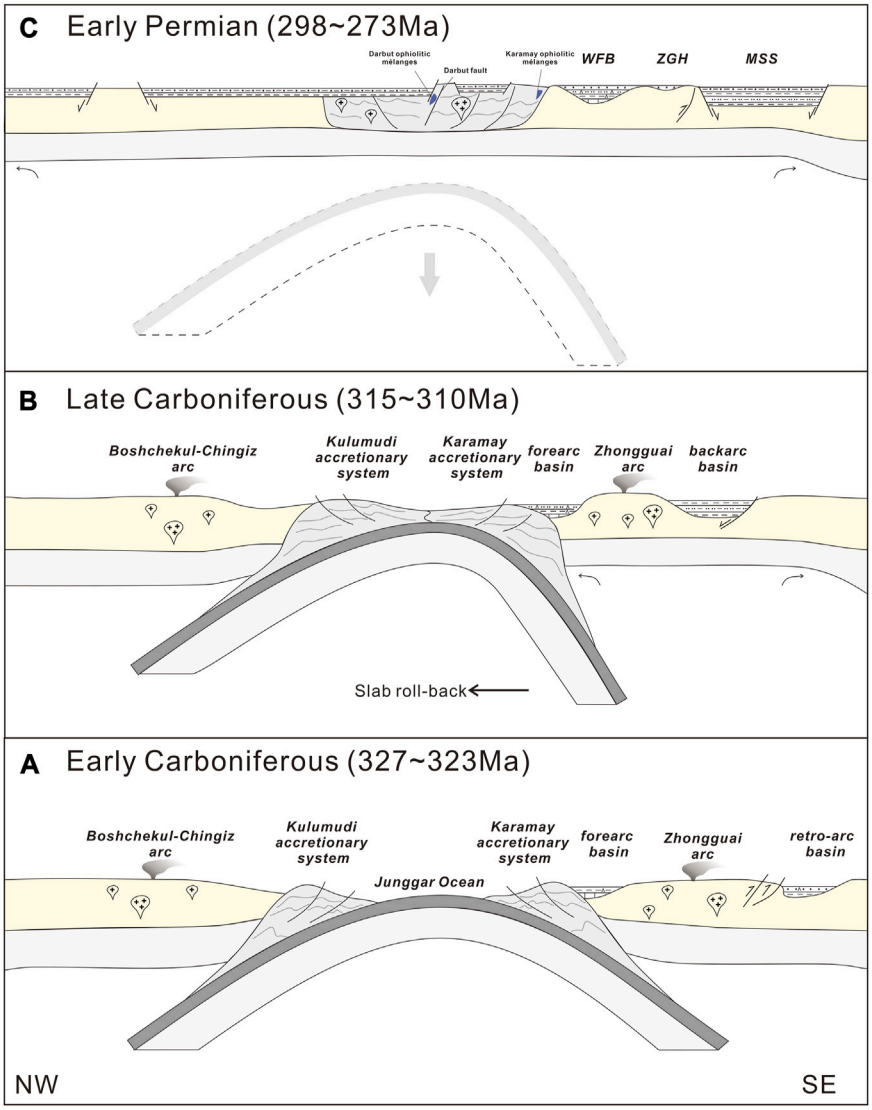

FIGURE 11
Schematic diagram showing the Carboniferous to Early Permian subduction–accretion processes and related basin evolution in the southern West Junggar region.

uncomformity between Carboniferous and Permian strata indicate that the southern West Junggar region may have evolved to a intraplate rift setting in the Early Permian (Figures 8C,E). Several lines of evidence support such inference. Firstly, the acidic volcanic rock samples show a clockwise trend from the Early Carboniferous through the Late Carboniferous to the Early Permian on the Rb vs. Y+Nb diagram (Figure 8F), indicating an evolutionary pattern from volcanic arc, through collision to post-collision (Wang et al., 2017). In addition, the Lower Permian deposition was mainly controlled by normal faults revealed by seismic reflection data and their sedimentary components are derived from the mixed source with mature continental continental quartz source signature (Figure 10). Moreover, the Early Permian strata was deposited in a terrestrial environment in contrast to those Carboniferous marine deposition. Another striking phenomenon is widespread distribution of the Early Permian A-type granites in the southern West Junggar region (Han and Zhao, 2018). These features point to a Carboniferous to Permian tectonic transition from subduction to post-collision, and together with the initial time of slab rollback and post-collisional granites, allow us to consider that the closure of the Junggar Ocean and resultant arc-arc collision occurred in the Late Carbonifeous (ca. 315–300 Ma), corresponding to a soft collision.

Based on the above discussions on tectonic-sedimentary evolution of the western Junggar Basin and magmatic distribution characteristics, an updated geodynamic evolutional model can be set up for the late Paleozoic subduction-collision processes in the southern West Junggar region. In the Early Carboniferous, double subduction of the Junggar Ocean resulted in the development of the Boshchekul-Chingiz and Zhongguai arcs. A forearc basin developed in the WFB in front of ZGH, and a series of thrust faults and related retro-arc basin were formed behind the Zhongguai arc (Li et al., 2017) (Figure 11A). During the Late Carboniferous, the rollback of southward subducted slab caused the lithosphere extension of the Zhongguai arc domain and

thus resulted in the development of the Mahu-Shawan backarc basin with upward fine-grained marine sediments, accompanied by massive rift-related structures and magmatism (Figure 11B). The Karamay and Kulumudi accretionary system may be amalgamated at this time and the Junggar Ocean began to be closed at ca. 315 Ma, which may last to latest Carboniferous. In the Early Permian, slab detachment induced asthenospheric upwelling and led to regional extension and rifting in the southern West Junggar region. This scenario is responsible for the generation of widespread 298-273 Ma A-type granites in this region and the Early Permian extensional structures recorded in the western Junggar Basin (Figure 11C), marking that the western Junggar Basin entered the intracontinental evolutionary stage.

6 Conclusion

(1) Three late Paleozoic tectono-stratigraphic units in the western Junggar Basin are identified, including Lower Carboniferous shallow-deep marine sequences, Upper Carboniferous coast-shallow marine sequences and Lower Permian terrestrial sequences.
(2) The southern West Junggar arc-basin system experienced the evolutionary history from Early Carboniferous retroarc basin to Late Carboniferous backarc basin to Early Permian intraplate rift basin, in response to the subduction-collision processes.
(3) The divergent double subduction resulted in the closure of the Junggar Ocean and the collision between Boshchekul-Chingiz arc and Zhongguai arc, and the oceanic basin was probably closed in the late Carboniferous.

Data availability statement

The original contributions presented in the study are included in the article/Supplementary Material, further inquiries can be directed to the corresponding author.

Author contributions

FY and HY: Conceptualization, Investigation, Methodology, Writing–original draft. JL: Conceptualization, Investigation, Writing–review and edit, Supervision. BB and HL: Funding acquisition. YW and XQ: Writing–review and edit; SL: Investigation. All authors contributed to the article and approved the submitted version.

Funding

This work was funded by the China Petroleum Major Science and Technology Project (2022DJ0507).

Acknowledgments

We appreciate the Editor and reviewers for their critical insight and constructive comments.

Conflict of interest

Authors FY, SL, YW, and XQ were employed by PetroChina Research Institute of Petroleum Exploration and Development; Author JL was employed by the PetroChina Tuha Oilfield Company; Authors BB and HL were employed by the PetroChina Xinjiang Oilfield Company.

The remaining author declares that the research was conducted in the absence of any commercial or financial relationships that could be construed as a potential conflict of interest.

Publisher's note

Supplementary material

The Supplementary Material for this article can be found online at: https://www.frontiersin.org/articles/10.3389/feart.2023.1237367/full#supplementary-material

References

An, F., and Zhu, Y. F. (2009). SHRIMP U-Pb zircon ages of tuff in Baogutu Formation and their geological significances. *Acta Petrol. Sin.* 25 (6), 1437–1445.

Belousova, E. A., Griffin, W. L., O'Reilly, S. Y., and Fisher, N. I. (2002). Igneous zircon: trace element composition as an indicator of source rock type. *Contributions Mineralogy Petrology* 143 (5), 602–622. doi:10.1007/s00410-002-0364-7

Busby, C. J., Smith, D., Morris, W., and Fackler-Adams, B. N. (1998). Evolutionary model for convergent margins facing large ocean basins; Mesozoic Baja California, Mexico. *Geology* 26, 227–230. doi:10.1130/0091-7613(1998)026<0227:EMFCMF>2.3.CO;2

Cawood, P. A., Kroener, A., Collins, W. J., Kusky, T. M., Mooney, W. D., and Windley, B. F. (2009). Accretionary orogens through Earth history. *Earth Accretionary Syst. Space Time* 318, 1–36. doi:10.1144/sp318.1

Cao, M., Qin, K., Li, G., Evans, N. J., Hollings, P., Jin, L., et al. (2016). Genesis of ilmenite-series I-type granitoids at the Baogutu reduced porphyry Cu deposit, western Junggar, NW-China. *Lithos* 246–247, 13–30. doi:10.1016/j.lithos.2015.12.019

Chen, B., and Zhu, Y. (2015). The origin of high-An plagioclase in diorite from Baikouquan, Xinjiang and its petrogenetic significance. *Acta Petrol. Sin.* 31 (2), 479–490. doi:10.00-0569/2009/025(06)-1437-45

Chen, S., Pe-Piper, G., Piper, D. J. W., and Guo, Z. (2014). Ophiolitic melanges in crustal-scale fault zones: implications for the Late Palaeozoic tectonic evolution in West Junggar, China. *Tectonics* 33 (12), 2419–2443. doi:10.1002/2013TC003488

Cullen, J. T., Field, M. P., and Sherrell, R. M. (2001). Determination of trace elements in filtered suspended marine particulate material by sector field HR–ICP–MS. *J. Anal. Atomic Spectrom.* 16, 1307–1312. doi:10.1039/b104398f

Dickinson, W. R. (1995). *Forearc basins*. Cambridge: Blackwell Science, 221–262.

Dickinson, W. R. (1974). Plate tectonics and sedimentation. *Soc. Econ. Paleontologists Mineralogists (SEPM) Special Publ.* 22, 1–27. doi:10.2110/pec.74.22.0001

Dickinson, W. R., and Seely, D. R. (1979). Structure and stratigraphy of forearc regions. *Am. Assoc. Petroleum Geol. Bull.* 63, 2–31. doi:10.1306/C1EA55AD-16C9-11D7-8645000102C1865D

Eizenhöfer, P. R., Zhao, G., Sun, M., Zhang, J., Han, Y., and Hou, W. (2015). Geochronological and hf isotopic variability of detrital zircons in paleozoic strata across the accretionary collision zone between the north China craton and Mongolian arcs and tectonic implications. *Bull. Geol. Soc. Am.* 127 (9-10), 1422–1436. doi:10.1130/b31175.1

Feng, J., Dai, J., and Ge, S. (2008). Structural evolution and pool-forming in Wuxia fault belt of Junggar Basin. *J. China Univ. Petroleum. Ed. Natrual Sci.* 32 (3), 23–29.

Feng, J., Dai, J., Qing, F., and Song, Y. (2019). Subsidence and sedimentary response of Wuxia foreland thrust belt in the northwestern margin of Junggar basin. *Acta Geol. Sin.* 93 (11), 2729–2741. doi:10.19762/j.cnki.dizhixuebao.2019096

Fildani, A., Hessler, A. M., and Graham, S. A. (2008). Trench-forearc interactions reflected in the sedimentary fill of Talara basin, northwest Peru. *Basin Res.* 30, 305–331. doi:10.1111/j.1365-2117.2007.00346.x

Fiske, R. S., Naka, J., Iizasa, K., Yuasa, M., and Klaus, A. (2001). Submarine silicic caldera at the front of the izu-bonin arc, Japan: voluminous seafloor eruptions of rhyolite pumice. *Geol. Soc. Am. Bull.* 113, 813–824. doi:10.1130/0016-7606(2001)113<0813:SSCATF>2.0.CO;2

Frey, F. A., Weis, D., Borisova, A. Y. U., and Xu, G. (2002). Involvement of continental crust in the formation of the cretaceous kerguelen plateau: new perspectives from ODP leg 120 sites. *J. Petrology* 43, 1207–1239. doi:10.1093/petrology/43.7.1207

Gao, S., He, Z., and Zhou, Z. (2006). Geochemical charcteristics of the Karamay granitoids and their significance in West Junggar, Xingjiang. *Xinjiang Geol.* 24 (2), 125–130.

Gorton, M. P., and Schandl, E. S. (2000). From continents to island arcs: A geochemical index of tectonic setting for arc-related and within-plate felsic to intermediate volcanic rocks. *Can. Mineral.* 38, 1065–1073. doi:10.2113/gscanmin.38.5.1065

Guo, L., Liu, Y., Wang, Z., Song, D., Xu, F., and Su, L. (2010). Anticancer activity and molecular mechanism of resveratrol-bovine serum albumin nanoparticles on subcutaneously implanted human primary ovarian carcinoma cells in nude mice. *Acta Petrol. Sin.* 26 (2), 471–477. doi:10.1089/cbr.2009.0724

Han, B., Guo, Z., Zhang, Z., Zhang, L., Chen, J., and Song, B. (2010). Age, geochemistry, and tectonic implications of a late Paleozoic stitching pluton in the North Tian Shan suture zone, western China. *Geol. Soc. Am. Bull.* 122 (3-4), 627–640. doi:10.1130/B26491.1

Han, B., Ji, J., Song, B., Chen, L., and Zhang, L. (2006). Late Paleozoic vertical growth of continental crust around the Junggar Basin, Xinjiang, China (Part I): timing of post-collisional plutonism. *Acta Petrol. Sin.* 22 (5), 1077–1086. doi:10.00-0569/2006/022(05)-1077-86

Han, Y., and Zhao, G. (2018). Final amalgamation of the tianshan and junggar orogenic collage in the southwestern central asian orogenic belt: constraints on the closure of the paleo-asian ocean. *Earth-Science Rev.* 186, 129–152. doi:10.1016/j.earscirev.2017.09.012

Hastie, A. R., Kerr, A. C., Pearce, J. A., and Mitchell, S. F. (2007). Classification of altered volcanic island arc rocks using immobile trace elements: development of the Th–Co discrimination diagram. *J. Petrology* 48, 2341–2357. doi:10.1093/petrology/egm062

He, D., Yin, C., Du, S., Shi, X., and Ma, H. (2004). Characteristics of structural segmentation of foreland thrust belts--A case study of the fault belts in the northwestern margin of Junggar Basin. *Earth Sci. Front.* 11 (3), 91–101.

Hoskin, P. W. O., and Schaltegger, U. (2003). The composition of zircon and igneous and metamorphic petrogenesis. *Zircon* 53, 27–62. doi:10.2113/0530027

Iizasa, K., Fiske, R. S., Ishizuka, O., Yuasa, M., Hashimoto, J., Ishibashi, J., et al. (1999). A Kuroko-type polymetallic sulfide deposit in a submarine silicic caldera. *Science* 283, 975–977. doi:10.1126/science.283.5404.975

Ingersoll, R. V. (1982). Initiation and evolution of the Great Valley forearc basin of northern and central California, U.S.A. *Geol. Soc. Lond. Spec. Publ.* 10 (1), 459–467. doi:10.1144/GSL.SP.1982.010.01.31

Ingersoll, R. V., and Schweickert, R. A. (1986). A plate-tectonic model for Late Jurassic ophiolite genesis, Nevadan Orogeny and fore-arc initiation, northern California. *Tectonics* 5 (6), 901–912. doi:10.1029/TC005i006p00901

Jahn, B. M., Wu, F. Y., and Chen, B. (2000). Granitoids of the Central Asian Orogenic Belt and continental growth in the Phanerozoic. *Trans. R. Soc. Edinburgh-Earth Sci.* 91, 181–193. doi:10.1017/s0263593300007367

Jahn, B., Windley, B., and Dobretsov, N. (2004). Phanerozoic continental growth in central Asia - Preface. *J. Asian Earth Sci.*, 23 (5), 599–603. doi:10.1016/S1367-9120(03)00124-x

Karig, D. E., and Sharman, G. F. (1975). Subduction and accretion in trenches. *Geol. Soc. Am. Bull.* 86 (3), 377–389. doi:10.1130/0016-7606(1975)86<377:SAAIT>2.0.CO;2

Khain, E. V., Bibikova, E. V., Salnikova, E. B., Kröner, A., Gibsher, A. S., Didenko, A. N., et al. (2003). The Palaeo-Asian ocean in the Neoproterozoic and early Palaeozoic: new geochronologic data and palaeotectonic reconstructions. *Precambrian Res.* 122 (1), 329–358. doi:10.1016/S0301-9268(02)00218-8

Kovalenko, V. I., Yarmolyuk, V. V., Kovach, V. P., Kotovet, A. B., Kozakov, I. K., Salnikova, E. B., et al. (2004). Isotope provinces, mechanisms of generation and sources of the continental crust in the Central Asian mobile belt: geological and isotopic evidence. *J. Asian Earth Sci.* 23 (5), 605–627. doi:10.1016/s1367-9120(03)00130-5

Kroner, A., Kovach, V., Belousova, E., Hegner, E., Armstrong, R., Dolgopolova, A., et al. (2014). Reassessment of continental growth during the accretionary history of the Central Asian Orogenic Belt. *Gondwana Res.* 25 (1), 103–125. doi:10.1016/j.gr.2012.12.023

Li, D. (2011). Geochemical Characteristics and Tectonic Settings of Carboniferous Volcanic Rocks from Junggar Basin, China. [Master thesis]. Beijing: China University of Geosciences.

Li, D., He, D., Lian, Y., Lu, Y., and Yi, Z. (2017). Structural evolution and late Carboniferous magmatism of the Zhongguai arc in the western Junggar Basin, Northwest China: implications for tectonic evolution of the Junggar Ocean. *Int. Geol. Rev.* 59 (10), 1234–1255. doi:10.1080/00206814.2016.1160801

Li, D., He, D., Yang, Y., and Lian, Y. (2014). Petrogenesis of mid-Carboniferous volcanics and granitic intrusions from western Junggar Basin boreholes: geodynamic implications for the Central Asian Orogenic Belt in Northwest China. *Int. Geol. Rev.* 56 (13), 1668–1690. doi:10.1080/00206814.2014.958766

Li, G., Li, Y., Xiang, K., Wang, R., Liu, J., Li, Z., et al. (2016). Sheep grazing causes shift in sex ratio and cohort structure of Brandt's vole: implication of their adaptation to food shortage. *J. Stratigr.* 40 (1), 76–84. doi:10.1111/1749-4877.12163

Liu, B., Han, B., Chen, J., Ren, R., Zheng, B., Wang, Z., et al. (2017). Closure Time of the Junggar-Balkhash Ocean: constraints From Late Paleozoic Volcano-Sedimentary Sequences in the Barleik Mountains, West Junggar, NW China. *Tectonics* 36 (12), 2823–2845. doi:10.1002/2017TC004606

Liu, B., Han, B., Xu, Z., Ren, R., and Chen, J. (2020). The Ediacaran to Early Palaeozoic evolution of the Junggar-Balkhash Ocean: a synthesis of the ophiolitic melanges in the southern West Junggar terrane, NW China. *Geol. J.* 55 (3), 1689–1707. doi:10.1002/gj.3475

Liu, J. (2015). Research on Permian in the Hala'alate Mountain, West Junggar. [Master thesis]. Beijing: Chang'an University.

Lu, Y. (2018). Permian Chronostratigraphic Framework and Sedimentary Filling Evolution in Mahu-shawan and Adjacent Area, Junggar Basin. [Master thesis]. Beijing: China University of Geosciences.

Marsaglia, K. M., and Ingersoll, R. V. (1992). Compositional trends in arc-related, deep-marine sand and sandstone: a reassessment of magmatic-arc provenance. *Geol. Soc. Am. Bull.* 104, 1637–1649. doi:10.1130/0016-7606(1992)104<1637:CTIARD>2.3.CO;2

Noda, A. (2016). Forearc basins: types, geometries, and relationships to subduction zone Dynamics. *Geol. Soc. Am. Bull.* 128 (5-6), 879–895. doi:10.1130/B31345.1

Pearce, J. A., and Peate, D. W. (1995). Tectonic implications of the composition of volcanic arc magmas. *Annu. Rev. Earth Planet Sci.* 23, 251–343. doi:10.1146/annurev.ea.23.050195.001343

Pearce, J. A., and Norry, M. J. (1979). Petrogenetic implications of Ti, Zr, Y and Nb variations in volcanic rocks. *Contrib. to Mineral. Petrol.* 69, 33–47. doi:10.1007/BF00375192

Pearce, J. A., Harris, N. B. W., and Tindle, A. G. (1984). Trace element discrimination diagrams for the tectonic interpretation of granitic rocks. *J. Petrol.* 25, 956–983. doi:10.1093/petrology/25.4.956

Peng, X., Li, Y., Li, W., Xiang, K., Li, G., and Li, Z. (2016). The Stratigraphic Sequence, Fossil Assemblage and Sedimentary Environment of Aladeyikesai Formation in Hala alate Mountain,West Junggar. *Xinjiang Geol.* 34 (3), 297–301.

Roser, B. P., and Korsch, R. J. (1988). Provenance signatures of sandstone-mudstone suites determined using discriminant function analysis of major-element data. *Chem. Geol.* 67 (1-2), 119–139. doi:10.1016/0009-2541(88)90010-1

Şengör, A., Natalin, B., and Burtman, V. (1993). Evolution of the Altaid tectonic collage and Palaeozoic crustal growth in Eurasia. *Nature* 364 (6435), 299–307. doi:10.1038/364299a0

Tang, G., Wang, Q., Wyman, D. A., Li, Z., Zhao, Z., Jia, X., et al. (2010). Ridge subduction and crustal growth in the Central Asian Orogenic Belt: evidence from Late Carboniferous adakites and high-Mg diorites in the western Junggar region, northern Xinjiang (west China). *Chem. Geol.* 277 (3), 281–300. doi:10.1016/j.chemgeo.2010.08.012

Tang, W., Wang, X., Guo, X., He, W., Tang, Y., Pe-Piper, G., et al. (2022). Late Carboniferous back-arc rifting in Junggar Basin, NW China: implication for the rapid continental growth in accretionary orogens. *Int. J. Earth Sci.* 111 (08), 2493–2518. doi:10.1007/s00531-022-02163-8

Tang, W., Zhang, Y., Pe-Piper, G., Piper, D. J. W., Guo, Z., and Li, W. (2021). Permian to early Triassic tectono-sedimentary evolution of the Mahu sag, Junggar Basin, western China: sedimentological implications of the transition from rifting to tectonic inversion. *Mar. Petroleum Geol.* 98, 104730–105124. doi:10.1016/j.marpetgeo.2020.104730

Taylor, S. R., and McLennan, S. M. (1985). *The continental crust: Its Composition and Evolution*. Oxford, UK: Blackwell Scientific Publications, 312.

Tong, L., Li, Y., Zhang, B., Liu, J., Pang, Z., and Wang, J. (2009). Zircon LA-ICP-MS U-Pb dating and geologic age of the Baogutu formation and andesite in the south of Daerbute faulted zone,western junggar. *Xinjiang Geol.* 27 (3), 226–230.

Wang, T., Wang, X., Guo, L., Zhang, L., Tong, Y., Li, S., et al. (2017). Granitoid and tectonics. *Acta Petrol. Sin.* 33 (5), 1459–1478. doi:10.00-0569/2017/033(05)-1459-78

Wilhem, C., Windley, B. F., and Stampfli, G. M. (2012). The Altaids of Central Asia: a tectonic and evolutionary innovative review. *Earth-Science Rev.* 113 (3-4), 303–341. doi:10.1016/j.earscirev.2012.04.001

Williams, I. S. (2001). Response of detrital zircon and monazite, and their U-Pb isotopic systems, to regional metamorphism and host-rock partial melting, Cooma Complex, southeastern Australia. *Aust. J. Earth Sci.* 48 (4), 557–580. doi:10.1046/j.1440-0952.2001.00883.x

Windley, B. F., Alexeiev, D., Xiao, W., Kroner, A., and Badarch, G. (2007). Tectonic models for accretion of the Central Asian Orogenic Belt. *J. Geol. Soc.* 164 (1), 31–47. doi:10.1144/0016-76492006-022

Winchester, J. A., and Floyd, P. A. (1977). Geochemical discrimination of different magma series and their differentiation products using immobile elements. *Chemical Geology* 20, 325–343. doi:10.1016/0009-2541(77)90057-2

Wu, F., Yang, Y., Mitchell, R. H., Bellatreccia, F., Li, Q., and Zhao, Z. (2010). *In situ* U–Pb and Nd–Hf–(Sr) isotopic investigations of zirconolite and calzirtite. *Chem. Geol.* 277, 178–195. doi:10.1016/j.chemgeo.2010.08.007

Xiang, K. (2015). Carboniferous Sedimentary Basin Analysis And Tectonic Significance in The Baogutu-Halaalate Mountain, Western Junggar. [Doctoral dissertation]. Xinjiang: Chang'an University.

Xiang, K., Li, Y., Li, Z., Wang, R., Yang, G., Duan, F., et al. (2015). LA ICP-MS Zircon Age and Geochemistry of the Aladeyikesai Formation Volcanic Rocks in the Halaalate Mountain of West Junggar, Xinjiang, and Their Tectonic Significance. *Acta Geol. Sin.* 89 (5), 843–855.

Xiang, K., Li, Y., Xu, L., Zhang, H., and Tong, L. (2013). The Definition of Chengjisihanshan Formation and Its Significances in Baijiantan Region, West Junggar, Xinjiang. *Northwest. Geol.* 46 (2), 63–68.

Xiao, W., Han, C., Yuan, C., Sun, M., Lin, S., Chen, H., et al. (2008). Middle Cambrian to Permian subduction-related accretionary orogenesis of Northern Xinjiang, NW China: implications for the tectonic evolution of central Asia. *J. Asian Earth Sci.* 32 (2-4), 102–117. doi:10.1016/j.jseaes.2007.10.008

Xiao, W., Huang, B., Han, C., Sun, S., and Li, J. (2010). A review of the western part of the Altaids: a key to understanding the architecture of accretionary orogens. *Gondwana Res.* 18 (2-3), 253–273. doi:10.1016/j.gr.2010.01.007

Xiao, W., Windley, B. F., Sun, S., Li, J., Huang, B., Han, C., et al. (2015). A Tale of Amalgamation of Three Permo-Triassic Collage Systems in Central Asia: oroclines, Sutures, and Terminal Accretion. *Annu. Rev. Earth Planet. Sci.* 43, 477–507. doi:10.1146/annurev-earth-060614-105254

Xu, X., He, G., Li, H., Ding, T., Liu, X., and Mei, S. (2006). Basic characteristics of the Karamay ophiolitic mélange, Xinjiang, and its zircon SHRIMP dating. *Geol. China* 33, 470–475.

Xu, Z., Han, B., Ren, R., Zhou, Y., and Su, L. (2013). Palaeozoic multiphase magmatism at Barleik Mountain, southern West Junggar, Northwest China: implications for tectonic evolution of the West Junggar. *Int. Geol. Rev.* 55 (5), 633–656. doi:10.1080/00206814.2012.741315

Yakubchuk, A. (2004). Architecture and mineral deposit settings of the Altaid orogenic collage: a revised model. *J. Asian Earth Sci.* 23 (5), 761–779. doi:10.1016/j.jseaes.2004.01.006

Yang, G., Li, Y., Gu, P., Yang, B., Tong, L., and Zhang, H. (2012). Geochronological and geochemical study of the Darbut Ophiolitic Complex in the West Junggar (NW China): implications for petrogenesis and tectonic evolution. *Gondwana Res.* 21, 1037–1049. doi:10.1016/j.gr.2011.07.029

Yang, H., Chen, L., and Kong, Y. (2004). A novel classification of structural units in Junggar Basin, Xinjiang. *Pet. Geol.* 25, 686–688.

Yi, Z., Huang, B., Xiao, W., Yang, L., and Qiao, Q. (2015). Paleomagnetic study of Late Paleozoic rocks in the Tacheng Basin of West Junggar (NW China): implications for the tectonic evolution of the western Altaids. *Gondwana Res.* 27 (2), 862–877. doi:10.1016/j.gr.2013.11.006

Yin, J., Long, X., Yuan, C., Sun, M., Zhao, G., and Geng, H. (2013). A Late Carboniferous-Early Permian slab window in the West Junggar of NW China: geochronological and geochemical evidence from mafic to intermediate dikes. *Lithos* 175, 146–162. doi:10.1016/j.lithos.2013.04.005

Yin, J., Yuan, C., Sun, M., Long, X., Zhao, G., Wong, K., et al. (2010). Late Carboniferous high-Mg dioritic dikes in Western Junggar, NW China: geochemical features, petrogenesis and tectonic implications. *Gondwana Res.* 17, 145–152. doi:10.1016/j.gr.2009.05.011

Zhan, Y., Hou, G., Hari, K. R., and Shu, W. (2015). Geochemical and isotopic constraints on the evolution of Late Paleozoic dyke swarms in West Junggar, Xinjiang, China. *J. Asian Earth Sci.* 113, 126–136. doi:10.1016/j.jseaes.2014.07.012

Zhang, C., and Huang, X. (1992). The ages and tectonic settings of ophiolites in West Junggar, Xinjiang. *Geol. Rev.* 38, 509–524. doi:10.16509/j.georeview.1992.06.007

Zhang, L. (2020). Geological Architecture, Sedimentary Filling, Formation and Mechanism of the Carboniferous Basin in the Junggar Area, NW China. [Doctoral dissertation]. Beijing: China University of Geosciences.

Zhang, L., Wang, G., Gao, R., Shen, T., Zong, R., and Yan, W. (2015). U-Pb Chronology of Detrital Zircons from the Carboniferous Sequences and its Geological Implications in West Junggar. *Geotect. Metallogenia* 39 (4), 704–717. doi:10.16539/j.ddgzyckx.2015.04.013

Zhang, P., Wang, G., Polat, A., Shen, T., Chen, Y., Zhu, C., et al. (2018a). Geochemistry of mafic rocks and cherts in the Darbut and Karamay ophiolitic melanges in West Junggar, northwestern China: evidence for a Late Silurian to Devonian back-arc basin system. *Tectonophysics* 745, 395–411. doi:10.1016/j.tecto.2018.08.018

Zhang, P., Wang, G., Polat, A., Zhu, C., Shen, T., Chen, Y., et al. (2018b). Emplacement of the ophiolitic melanges in the west Karamay area: implications for the Late Paleozoic tectonic evolution of West Junggar, northwestern China. *Tectonophysics* 747, 259–280. doi:10.1016/j.tecto.2018.08.019

Zhang, P., Wang, G., Shen, T., Polat, A., and Zhu, C. (2021). Paleozoic convergence processes in the southwestern Central Asian Orogenic Belt: insights from U-Pb dating of detrital zircons from West Junggar, northwestern China. *Geosci. Front.* 12 (2), 531–548. doi:10.1016/j.gsf.2020.07.015

Zhang, Y., and Guo, Z. (2010). New constraints on formation ages of ophiolites in northern Junggar and comparative study on their connection. *Acta Petrol. Sin.* 26 (2), 421–430. doi:10.00-0569/2010/026(02)-0421-30

Zheng, B., Han, B., Liu, B., and Wang, Z. (2019). Ediacaran to Paleozoic magmatism in West Junggar Orogenic Belt, NW China, and implications for evolution of Central Asian Orogenic Belt. *Lithos* 338, 111–127. doi:10.1016/j.lithos.2019.04.017

Zhu, D., Zhao, Z., Niu, Y., Dilek, Y., Wang, Q., Ji, W., et al. (2012). Cambrian bimodal volcanism in the Lhasa Terrane, southern Tibet: record of an early Paleozoic Andean-type magmatic arc in the Australian proto-Tethyan margin. *Chem. Geol.* 328, 290–308. doi:10.1016/j.chemgeo.2011.12.024

Zhu, Y., Chen, B., and Qiu, T. (2015). Geology and geochemistry of the Baijiantan-Baikouquan ophiolitic melanges: implications for geological evolution of west Junggar, Xinjiang, NW China. *Geol. Mag.* 152 (1), 41–69. doi:10.1017/S0016756814000168

Zhu, Y., Chen, B., Xu, X., Qiu, T., and An, F. (2013). A new geological map of the western Junggar, north Xinjiang (NW China): implications for Paleoenvironmental reconstruction. *Episodes* 36 (3), 205–220. doi:10.18814/epiiugs/2013/v36i3/003

Zhu, Y., and Xu, X. (2006). The discovery of Early Ordovician ophiolite melange in Taerbahatai Mts., Xinjiang, NW China. *Acta Petrol. Sin.* 22 (12), 2833–2842. doi:10.00-0569/2006/022(12)-2833-42